Rain-out investigation: initial droplet size measurement

Jean-Pierre Bigot[*,a]; Abdellah Touil[a]; Patrick Bonnet[b]; Jean-Marc Lacôme[b]

[a]*Ecole nationale supérieure des mines de Saint-Etienne, 158 cours Fauriel, F-42023 St-Etienne cedex 2*

[b]*INERIS, B.P. 2, F-60550 Verneuil en H datte*

Abstract

Droplet size distribution inside water flashing jets and corresponding rainout fraction were measured. Mass distribution showed that a few droplets are "large" (> 150 μm) and count for more than 85 % of the liquid mass in the jet because of their large individual mass. This could be due to incomplete thermal fragmentation. It could explain the rain-out falling near the orifice or pipe exit.

Keywords: rain-out, loss of containment, flashing liquid jets, thermal fragmentation, droplet size distribution

1. Introduction

The rain-out problem is part of the loss of containment scenario about liquefied gases reservoirs: how much of the released liquid phase will fall on the ground? This fraction will not directly participate to the toxic or flammable cloud.

Experimental data about this topic are seldom (Johnson 1999, Hocquet 2002). Models are either not sufficiently validated because of this lack of experimental data or even not in good agreement with the existing ones (Wheatley 1987, Ianello 1989, Epstein 1990, Papadourakis 1991, UDM, Johnson 1999).

A former work (Hocquet 2002) showed that rain-out forms a few meters down-stream the accidental breach *under* the horizontal aerosol. However literature predicts small droplets (d_d < 150 μm) will be formed through the thermal fragmentation mechanism (Brown 1962, Bushnell 1968, Gooderum 1969, Lienhard 1970, Oza 1983-1984, Razzaghi 1989, Reitz 1990Park 1994, Ramsdale 1998, Witlox 2000-2001). Such small droplets would normally be

* corresponding author. *Tel. +33 (0)4 77 42 00* 29; fax : +33 (0)4 77 42 49 96 94; bigot@emse.fr

entrained by the aerosol. The aim of this work is to understand how this non homogeneous behaviour can occur.

2. Experimental

We used two different experimental set-ups in order to measure drop sizes, temperature and rainout fraction for known initial conditions T_{res} and P_{res}. Both set-ups used the same test sections. The tested fluid was water.

2.1. Test sections: orifices and pipes

We used both stainless steel orifices and pipes (fig. 1). The 2 mm inner diameter orifice (D2) and pipe (D2L100) where mainly used. But some experiments were conducted with D5 and D8 orifices, D5L250 and D8L400 pipes.

2.2 Rainout, mass flow rate and jet temperature measurements

The experimental set-up for these measurements is mainly composed of an upstream tank, the test section, jet temperature probes and rainout capture basins (fig. 2. & 3.).

The up-stream tank is intended to maintain the tested fluid in a stable thermodynamic state all along an experiment. It consists of a jacketed stainless steel column (4.5 m high, .257 m inner diameter, .233 m^3 volume). It allows for a few minutes steady-state experiments. We experimented up to Po = 1.1 MPa and To = 350K (170°C). Heat is provided to the tested fluid by a 30 kW electrical heater through oil flowing in the jacket. A .12 m thick rock-wool insulation around the tank allows for a heat transfer coefficient to the surroundings as low as h = .5 W/m^2K. Tested fluid is circulated (.7 m3/h) from the bottom of the tank to the upper gas phase. This allows obtaining $\pm$ .1 K temperature uniformity for the tested fluid inside the tank. Pressure at the test section level is maintained constant (within ± 2 kPa) owing to loop controlled nitrogen introduction.

Jet temperature is measured both on its axis and just above the capture basins through 20 equally spaced (1 m) Pt temperature probes. Time constant for these probes induces a ± .75K measurement uncertainty.

Mass flow rate through the test section is measured by comparing the change of the pressure head above the test section during and experiment to the change when a known amount of liquid is added.

15 capture basins (1m * 2 m or 1 m * 1 m) allow rain-out water capture (fig. 2. & 3.). Water captured in each capture basin is gravity transferred to a smaller container and then weighted. Ratio of mass in one capture basin to the total mass released from the upstream tank (obtained from mass flow rate and experiment duration measurement) is a measure of the rainout density function (± 1 % accuracy).

2.3 Droplet velocity and size measurements

The experimental set-up for these measurements is mainly composed of another up-stream tank, the same test sections and a PDPA system. The test section is connected to the up-stream tank through a 3 m long, .013 m inner diameter, void heat insulated flexible hose (fig. 4. & 5.).

This up-stream tank allows the same initial thermodynamic conditions (1.1 MPa, 350K) to be obtained as the other one. It is sphere shaped. The useful volume is approximately 1. m^3. Internal electrical heating is provided, as well as N2 inlet. Both are manually monitored leading to a typical chang of ± 10^4 Pa and ± .5 K just up-stream the test section during an experiment.

A DANTEC Dual-PDPA[1] allows local measurements (typical 1 mm^3 volume) of both two components of individual droplet velocity and diameter. Statistics about droplet diameter lead to size distribution.

The measurement volume can be moved in the three directions (2.7 m * .6 m * 1.5 m). Thus different measurement locations can be tested during the same experiment. We generally covered the vertical plane which includes the jet axis as described in fig. 6.

2.4. Droplet size measurement accuracy

The PDPA stops when 3000 measures are collected or after 5 seconds if less than 3000 measures were collected. At 25 and 50 mm downstream of the D2L100 pipe, the apparatus only detects a few droplets (260 et 193 respectively) during the 5 s which are allowed. The difficulty is probably linked to the optical density of the jet in this region : beams generally cannot cross the jet without being refracted. At intermediate distances (generally comprising 200 mm downstream the orifice or pipe) 3000 droplets are measured in less than 5 s.

The number of measures during 5 s decreases again farther than 4 or 600 mm. The main reason is probably the decrease in the density of the jet when going farther and farther from the source. Sometimes droplets impact the lenses of the apparatus…

We thus decided to use a distance of 200 mm on the jet axis as our reference location. Another justification for this location is that the change in the size distribution is very important in the first few centimetres and clearly slower after 200 to 400 mm.

We estimate the Sauter mean diameter from the sample collected by the PDPA. This sample has to be large in order that the estimated value is close to the actual one. Most of the measured droplets are "small droplets" ($d_d < 150\ \mu m$).

[1] 2 300 mW argon lasers in two orthogonal planes, 60X Fiber Flow series, 57X80 and 58N81 detectors, BSA P70 electronic module, mask C.

Figure 7. shows that estimated mean value for the small droplets is correct within a few micrometers when the sample has 3000 droplets. The "larger drops" play a predominant role when estimating d_{32} for the whole population because of their large V/S ratio. But these drops are relatively few among the whole population (~ 40 à 50 % at T_{res} ~ 105°C, 3 to 10% when T_{res} ~ 165°C). When the apparatus stops because he counted 3000 droplets, the sample of larger ones is still limited (100 and 300 droplets for the two situations depicted on figure zxy). It is the reason why the convergence is slower. We can estimate the uncertainty as:

± 100 μm for a sample of 3000 droplets at high temperature (T_{res} ~165°C) when the number of large droplets is the lower.

± 20 μm for a sample of 6000 droplets at high temperature

3. Results and discussion

Tested reservoir conditions are summarized in figures 8. (pipes) and 9. (orifices)

3.1. Flow type

Figure 10. shows mass velocity (W/A) data for *orifices* (A is the nominal section of the orifice) versus relative reservoir pressure. Lines show Bernoulli equation flow ($G = CD \sqrt{2\rho_l (P_{res} - P_a)}$) for different discharge coefficient values. There is a very good coincidence if discharge coefficient is fitted (C_D = 0.67 for D2, CD = 0.70 for D5). This shows that *observed flows are purely liquid,* as is expected for ideal orifices. Using "standard" discharge coefficient (C_D = .61) leads to 10 or 15% mass flow rate uncertainty. But actual industry problems will never be concerned by ideal orifices and comparison with models do not necessitate a better level of accuracy.

Mass flow rates from experiments with *pipes* at temperatures lightly higher than the boiling one (up to 395K) show a complete agreement (± 5%) with purely liquid flow assumption (constant linear friction coefficient: $\lambda_c = 0{,}016$). Figure 11. represents mass

velocities measured at higher temperatures (T > 395 K). The agreement with the Bernoulli-like approach (or Lackmé approach: $G = \sqrt{2\rho_l(P_{res} - P_{sat}(T_{res}))}$) is quite good. It is better than using a model for initially saturated fluid (Fauske 1985 for example) even at low sub-cooling (1 to 2.10^4 Pa here). This means that the *flow is liquid in the main part of the pipe but there is some form of vaporisation just up-stream its end.*

3.2. Rain-out measurements

Figure 12. et 13. show the spatial distribution for the rain-out downstream both orifice and pipes experiments. They are very similar one to the other (for similar reservoir conditions) as opposed to the completely different behaviour downstream a longer pipe (D8L4000; Hocquet 2002). This suggests a large influence of pressure gradient $(P_{res} - P_{sat}(T_{res}))/L$ on two-phase flow structure inside the pipe. The 2-phase flow region is much shorter for the shorter pipe(fig. 14.), so that almost *no internal fragmentation* can occur (when AP/L > 1 MPa/m instead of AP/L < .1 MPa/m). This leads to the small pipe (D2L100) behaving like an orifice. *Our pipe measurements are representative of such highly sub-cooled flows only.*

Figures 15. and 16. show the global rain-out we measured versus reservoir temperature T_{res}. Two important features of these data are that there is *no significant influence of the reservoir pressure on rainout fraction* and that *data after a pipe are not so different from ones obtained after an orifice.* The agreement is good with data from the CCPS experiments (Johnson 1999).

3.3. Droplet diameter measurements; Number and mass distribution

Figures 17. (D2L100 pipe) and 18. (D2 orifice) show that all distributions have a peak in the [0, 150 μm] range, whatever T_{res} et P_{res},. The shape of this peak is similar to what was reported in the literature (Brown 1962, Bushnell 1968, Gooderum 1969, Lienhard 1970, Oza

1983-1984, Razzaghi 1989, Reitz 1990Park 1994, Ramsdale 1998, Witlox 2000-2001), qualitatively near a log-normal or a Rosin–Rammler distribution. Our measurements show that another population exists. At low temperature (T_{res} = 80°C, 104° C and 124°C), one observes a quasi-uniform distribution (almost the same number of droplets in each size class) up to 600 um (PLDA limit for the used configuration). At higher temperatures (136 to 167°C) a few droplets with diameter larger than 150 urn still exist, most of them between 200 et 300 μm .

Droplet mass is more important than droplet number as far as rainout phenomenon is concerned. This led us to represent size distribution using the mass probability density function. Figures 19. and 20. show a completely different trend. *The "small droplets" (d_g< 150μm),* which represent the larger number (T > 90 % for T_{res} > 136°C and still T > 45 % for T_{res} ≥ 80°C) *only represent 0,5 to 17 % of the mass! And the large ones count for the complement, i.e. 83 to 99,5 % of the mass!* The mass fraction for the « large droplets » in our temperature range is always the larger one. It represents almost all the mass when T_{res} < 125°C. It then slowly decreases to approximately 85% at T_{res} ~ 165°C (fig. 21.). The sensitivity of this fraction to the pressure seems to be low, probably lower than the measurement uncertainty.

It seems to us that such a large fraction of large drops was never mentioned in the literature up to now especially in case of thermal fragmentation. This could be due to experimental considerations : in order to obtain best measurements where most of the droplets are present, it is often better to limit the measurement range. With our apparatus configuration the signal was very weaker in the [0, 600 um] (mask C) range than in the [0, 200 um] (mask A) range. Another reason is that most of the literature is devoted to very small orifices, generally less than 500 um (Diesel injection for example).

3.4. Change with P_{res} et T_{res}

The distribution which appeared as quasi-uniform in number at the lower temperatures (T_{res} < 125°C) appears increasing with diameter when represented in mass because mass increases as diameter to the cube. The mass representation shows that *the same distribution still exists at the higher temperatures for the larger droplets* (we define them from the histograms as : d_d >325 μm). Further observing the mass histograms we are tempted to distinguish a third population: a peak between *150* μm *and 325* μm is almost absent at the lower temperatures (T_{res} < 105°C), but grows when temperature increases. When temperature is higher than T_{res} = 136°C its mass is more than that of « small droplets ». These comments apply to both D2 orifice and D2L100 pipe.

Histogram at 80°C (fig. 18.) can only be understood as resulting from pure mechanical fragmentation. It consists of a quasi-uniform distribution between 0 and 600 um, plus a peak of very fine droplets (around d_d = 15 um). The histograms at 104°C or 124°C are qualitatively similar. The only difference is that the peak moved to lightly larger diameters. Fragmentation at such T_{res} probably still corresponds to essentially mechanical fragmentation.

Thermal fragmentation is thus not the only one which can form very fine droplets (d_d < 50 um). Thus we cannot decide if the peak of "small droplets" (d_g < 150 urn, more than 90 % of the droplets at high temperature) has a thermal or mechanical origin. There is perhaps superimposition of a mechanical peak and a thermal one at lightly larger diameters. The growth of the thermal peak could eventually explain that the global peak moves towards slightly larger diameters when temperature increases.

The "medium" peak (150 μm < d_g <325 μm) is almost absent at the lower temperatures (fig 19. et 20.) (T_{res} < 125°C). It becomes visible at 136°C and is larger at T_{res} ~ 165°C. This leads us *to associate it with thermal fragmentation.* The *"larger drops"* would be a remaining part of the primary fragmentation which would *not have undergone secondary one.*

This would mean that the thermal fragmentation would only concern a fraction of the liquid, with the "larger drops" staying in a meta-stable state ! Fig 21. shows that the mass fraction for these droplets is very high, even if it decreases when temperature increases: 90 % at T_{res} ~ 105°C, still ~ 60 % at T_{res} ~ 165°C. Perhaps the number of nuclei is not large enough for thermal fragmentation to be complete. This type of fragmentation would be more intensive at higher temperatures because more nuclei would be activated

3.5. Axial change of mean size

Fig. 22. and 23. represent the probability density function data at different locations downstream the orifice or pipe. Fig. 24. and 25. show the corresponding mass distributions.

When measures are available very near the pipe or orifice (pipe D2L100 at 124°C and 8,1 bar ; orifice D2 at 163, 4°C and 8,2 bar), they often show a quasi-uniform distribution over the whole measured range. As far as measures can be considered as reliable at these distances, this would mean that a very fast *primary fragmentation* mechanism would exist which would not depend very much on geometry (pipe/orifice) nor on reservoir pressure or temperature.

The number fraction of « small droplets » (d_d < 150 um) increases rapidly: from ~ 20 % at 5 mm to between 80 and 90 % at 30 mm. The maximum is reached between 200 and 400 mm down-stream the orifice or pipe (fig. 22.). Meanwhile a peak between 150 urn and 325 um appears on the mass histograms. This means that there exists at least one *external secondary mechanism* which breaks the droplets mainly in the first few centimetres, and continues during 200 to 400 mm.

The Sauter mean diameter decreases when the number of « small droplets » increases (from pipe exit to ~ 200-400 mm down-stream; fig. 26. & 27.). It can then increase when their relative weight decreases (farther than 200 to 400 mm). Their relative weight decreases slower when temperature is lower, which could explain that the trend for d_{32} to increase comes

farther. Note that the observed diameter increase is generally smaller than the uncertainties but the trend is observed for all the experiments.

4. Conclusion

Two pilot scale experimental set-up allowed us to characterize flashing water jets. We measured mass flow rate, initial droplet size and velocity distributions, plus spatial distribution of rain-out. Test sections were both orifices and pipes, mainly 2 mm inner diameter.

Mass flow rate measurements and spatial distribution of rain-out showed that almost no internal fragmentation in the pipe occurs when reservoir sub cooling is large enough ($\Delta P / L > 1$ MPa / m). In such conditions both pipes and orifice exhibit the same jet behaviour (rain-out fraction and rainout spatial distribution).

Reservoir pressure (P_{res}) has not a significant influence on total rain-out fraction as compared to reservoir temperature T_{res}.

All droplet size distributions exhibit a peak in the [0 ÷ 150 μm] range as described in the literature. But some larger droplets are also detected. These last ones count fore more than 85 % of the liquid mass even when they count for less than 10 % of the droplets number!

Quasi-uniform droplet size distribution (almost the same number of droplets in each size class) very near pipe or orifice could result from a very quick *primary fragmentation mechanism.*

The "small droplets" (d_d < 150 (am) form mainly in the few first centimetres with the maximum number reached between 200 and 400 mm downstream the orifice or pipe. Mass histograms show that another peak forms between 150 and 325 μm. These two peaks mean that an *external secondary fragmentation mechanism* exists.

The former observations lead to the following scheme:

- a primary mechanical fragmentation mechanism exists whatever the conditions (orifice or pipe, high or low temperature). It curiously leads to a quasi-uniform distribution of the droplet diameters,
- some of these droplets undergo very rapidly (mostly less than 10 mm) a secondary mechanical fragmentation and probably a thermal fragmentation. This leads to a population of "small droplets" (d_d < 150 urn). This mechanism is stronger at the higher temperatures.
- When temperature increases another fraction of the droplets is concerned with thermal fragmentation. This leads to the "medium droplets" (150 um < dd < 325 um).
- An important residual quantity of droplets do not undergo secondary fragmentation. They constitute the "large droplets" population » (325 um < dd < 625 um).

The large mass fraction of large droplets (d_d > 150 μm).could be an explanation for our former observation that rain-out is heterogeneous in nature (Hocquet 2002) : it is composed of droplets which fall *under* the almost horizontal two phase jet. Our next aim will be to prove that such size distributions can be a basis in order to improve rain-out prediction models. Future work will also have to take into account near saturation reservoir conditions and fluids other than water.

References

Brown, R., & York, J.L. (1962). Sprays formed by flashing liquid jets. *American Institute of Chemical Engineers Journal*, Vol. 8, n°. 2, p. 149-153.

Bushnell, D.M., & Gooderum, P.B. (1968). Atomisation of superheated Water jets at low ambient pressures, *A.I.A.A,* Vol. 5, n°. 2, 231-232.

Epstein, M., Fauske, H.K., & Hauser, G. M. (1990). A model of the dilution of a forced two-phase chemical plume in a horizontal wind. *Journal of Loss Prevention Process Industries,* Vol. 3, n°. 3, 280-290.

Fauske, H.K. (1985). Flashing flows or: some practical guidelines for emergency releases. *Plant/Operations Progress,* Vol. 4, n°. 3, 132-4.

Gooderum, P.B., & Bushnell, D.M. (1969). Measurement of Mean Drop Sizes for Sprays from Superheated Water jets, *Journal of Spacecraft and Rockets,* Vol. 6, n° 2, 197-198.

Hocquet, J., Adrian, J.-C., Godeau, M., Marchand, V., & Bigot, J.-P. (2002). Loss of containment : experimental aerosol rain-out assessment. *Journal of Hazardous Materials,* V 93, 67-76.

Ianello, V., Rome, P.H., Wallis, G.B., Diener, R., & Schreiber, S. (1989). Aerosol research program: improved source term définition for modelling the ambient impact of accidental release of hazardous liquids, *Proc. 6th Int. Symp. Loss Prevention and Safety Promotion in the Process Industries,* Oslo, 58-1, 58-29.

Johnson, D.W., & Woodward, J.L. (1999). RELEASE A model with data to predict aerosol Rainout in accidental Releases, *Center for Chemical Process Safety, AIChE.*

Lienhard, J.H., & Day, J.B. (1970). The break-up of superheated liquid jets. *Journal of. Basic Engineering.*

Oza, R.D., & Sinnamon, J.F. (1983). An Experimental and Analytical Study of Flash-boiling Fuel Injection. *SAE Paper.*

Oza, R.D. (1984). On the Mechanism of Flashing Injection of Initially Sub-cooled Fuels. *Journal of Fluids Engineering,* Vol. 106, 105-109.

Papadourakis, A., Caram, H.S., & Barner, C.L. (1991). Upper and lower bounds of droplet evaporation in two-phase jets, *Journal of Loss Prevention Process Industries,* Vol. 4, 93-101.

Park, B.S., & Lee, S.Y.(1994). An experimental investigation of the flash atomisation mechanism, *Atomisation and Sprays*, Vol. 4, n°. 2, 159-179.

Ramsdale, S.A. (1998). Droplet formation and rain-out from two phase flashing jets. *Rapport AEAT-2124 Issue 1.*

Razzaghi, M. (1989). Droplet size estimation of two phase flashing jets. *Nucl. Eng. Des,* Vol. 114, 115-124

Reitz, R.D. (1990). A Photographic Study of Flash-Boiling Atomisation. *Aerosol Science and Technology*, Vol. 12, 561-569.

Wheatley, C.J. (1987). Discharge of liquid ammonia to moist atmospheres, survey of experimental data and model for estimating initial conditions for dispersion calculations, *SRD, R 410.*

Witlox, H.W.M., & Holt, A. (2000). Unified Dispersion Model. *Technical Reference Manual*, Version 6.0, DNV. London.

Witlox, W.M., & Bowen. P.J. (2001). Flashing liquid jets and two-phase dispersion. *HSE Books a review.*

Fig. 1.: scheme of the test sections (orifices and pipes)

Fig 2. : scheme of the set-up for rain-out measurements

Fig 3. : photograph of the jet with the capture basins .

Fig. 4.: scheme of the set-up for droplet size measurement

Figure 5 : Photograph of test section and PDPA (no jet).

Fig. 6 : typical PDPA measurement locations

Fig 7.: d32 measurement accuracy versus droplet number (small droplets ; whole population).

fig. 8.: Experimental reservoir conditions. Water jets from orifices.

fig. 9.: Experimental reservoir conditions. Water jets from pipes.

Figure 10. : Mass velocity versus relative reservoir pressure (orifices)

Fig 11. : mass velocity versus (P_{res} - P_{sat} (T_{res})) (pipes)

Fig 12. : Spatial distribution of rain-out (D2 orifice).

Fig 13. : Spatial distribution of tain-out (D2L100 pipe).

Fig. 14. : influence of pressure gradient on internal 2-phase flow structure

Fig. 15. : rain-out fraction versus reservoir temperature (pipes).

Fig. 16. : rain-out fraction versus reservoir temperature (orifices).

Fig. 17. : Number size distribution at different reservoir conditions
(200 mm down-stream from D2L100 pipe)

Fig. 18. : Number size distribution at different reservoir conditions
(200 mm down-stream from D2 orifice)

Fig. 19. : mass size distribution at different reservoir conditions
(200 mm down-stream from D2L100 pipe)

Fig. 20. : mass size distribution at different reservoir conditions
(200 mm down-stream from D2 orifice)

Fig. 21. : mass % of large droplets versus reservoir temperature

Fig. 22: number size distribution at different locations

(D2L100 pipe, T_{res} = 397K; P_{res} = .82 MPa)

Fig. 23: number size distribution at different locations

(D2 orifice, T_{res} = 437K; P_{res} = .82 MPa)

Fig. 24: mass size distribution at different locations

(D2L100 pipe, T_{res} = 397K; P_{res} = .82 MPa)

Fig. 25: mass size distribution at different locations

(D2 orifice, T_{res} = 437K; P_{res} = .82 MPa)

Fig. 26. : Change of mean SAUTER with distance from the pipe

Fig. 27. : Change of mean SAUTER with distance from the orifice

D2, D5, D8 D2L100, D5L250, D8L400

Fig. 1.: scheme of the test sections (orifices and pipes)

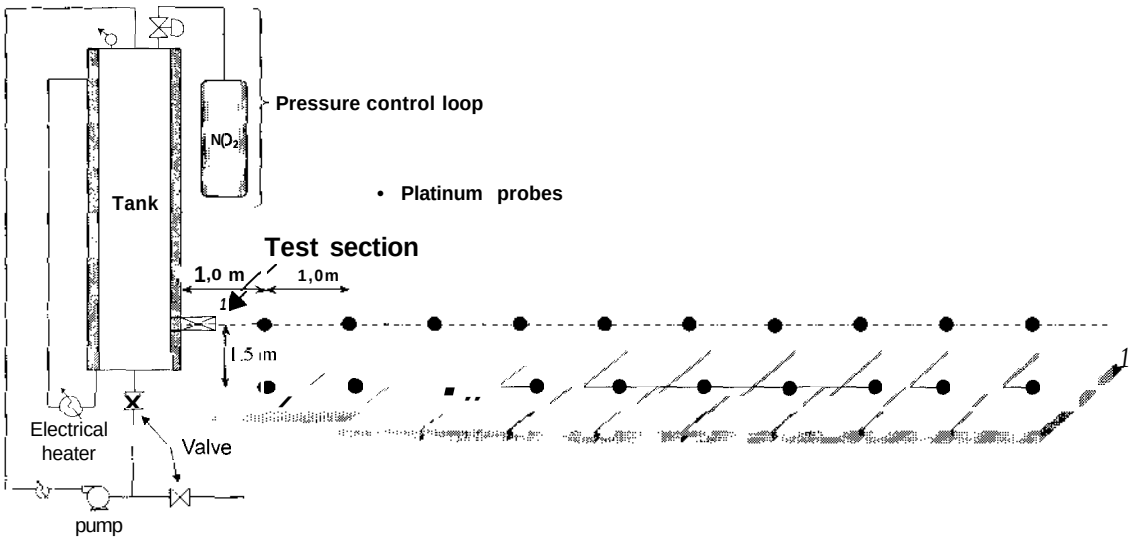

Fig 2. : scheme of the set-up for rain-out measurements

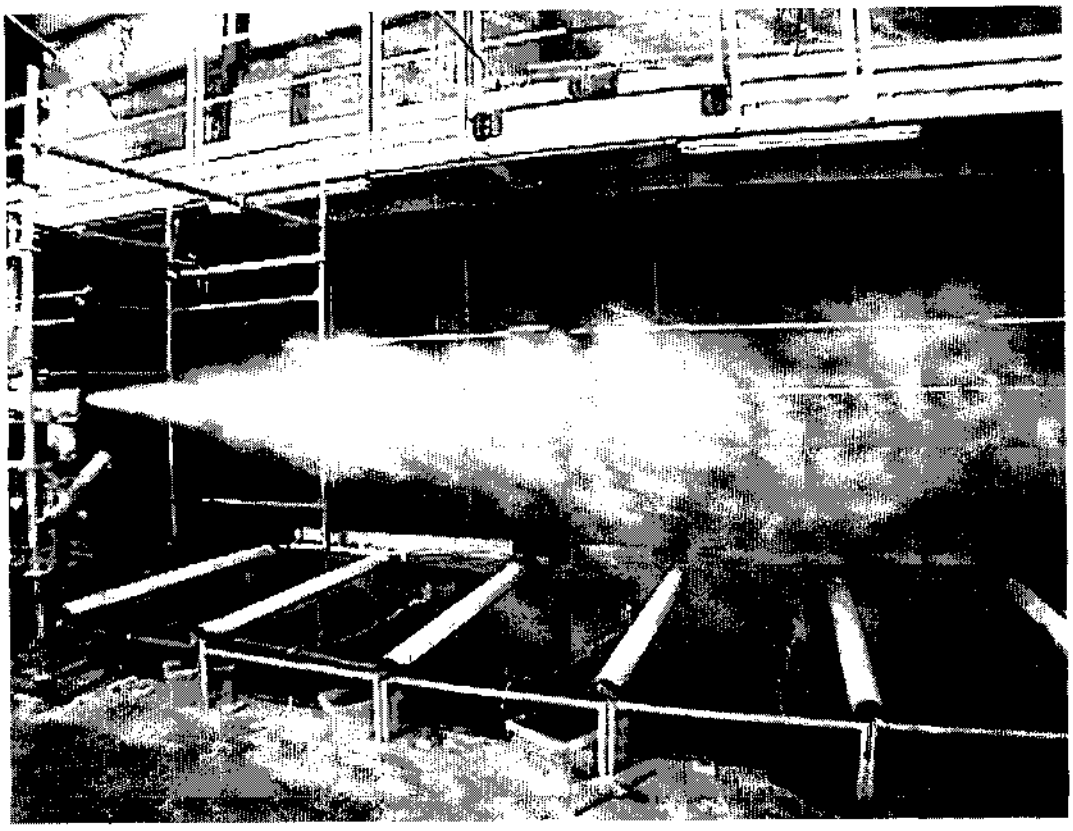

Fig 3. : photograph of the jet with the capture basins .

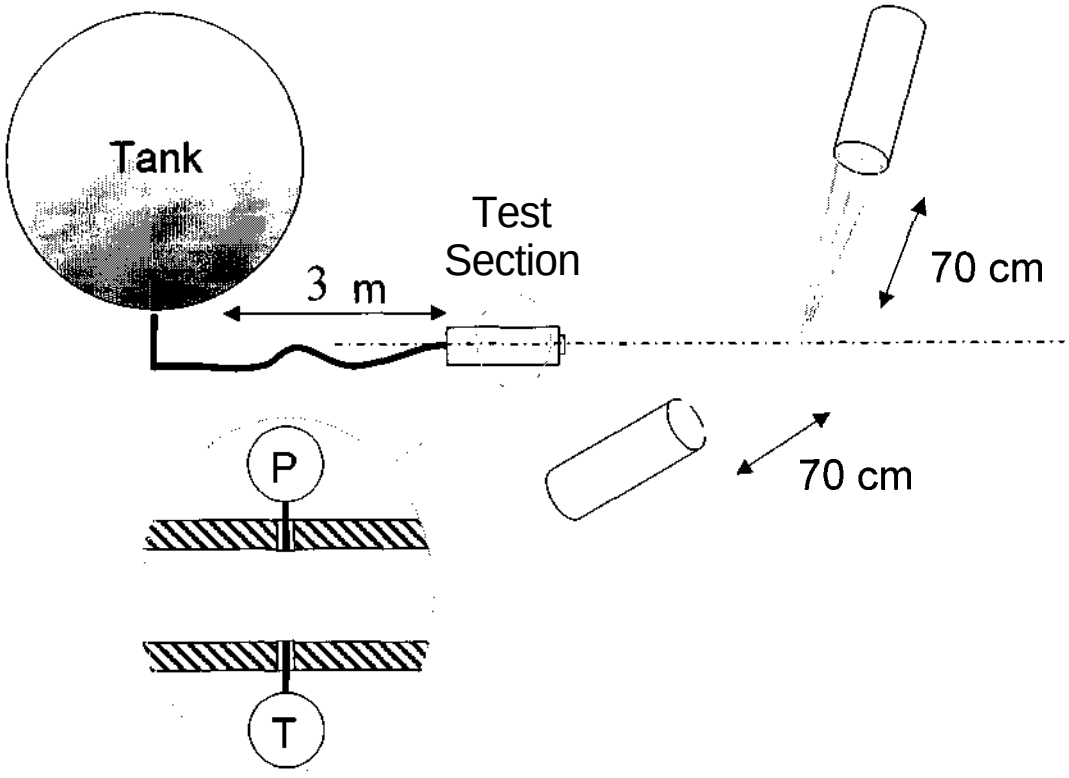

Fig. 4.: scheme of the set-up for droplet size measurement

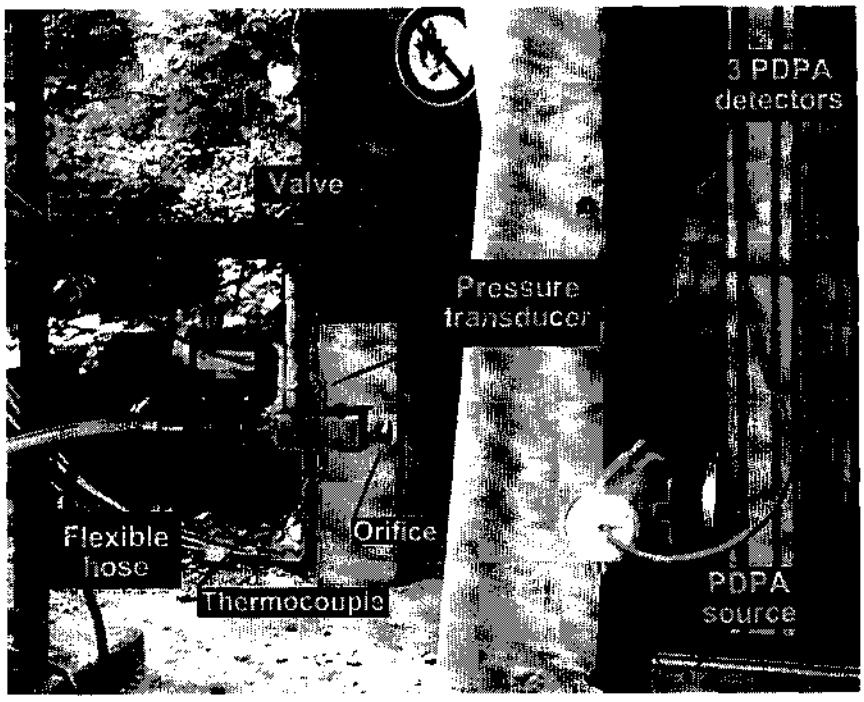

Figure 5 : Photograph of test section and PDPA (no jet).

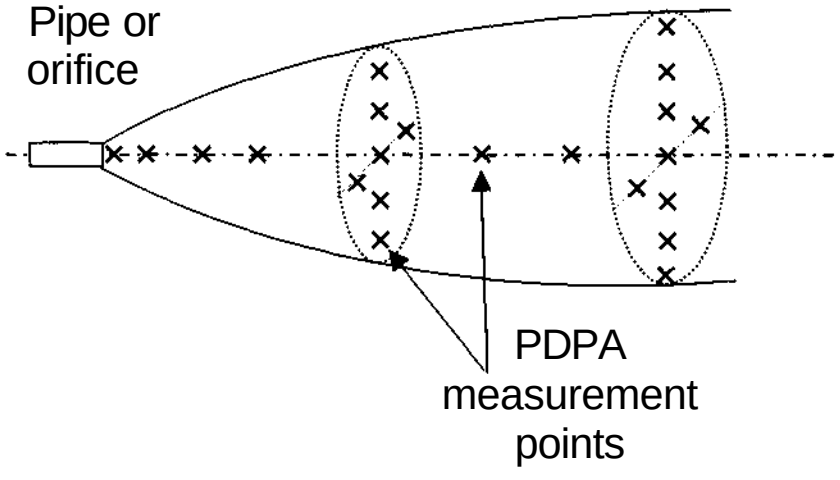

Fig. 6 : typical PDPA measurement locations

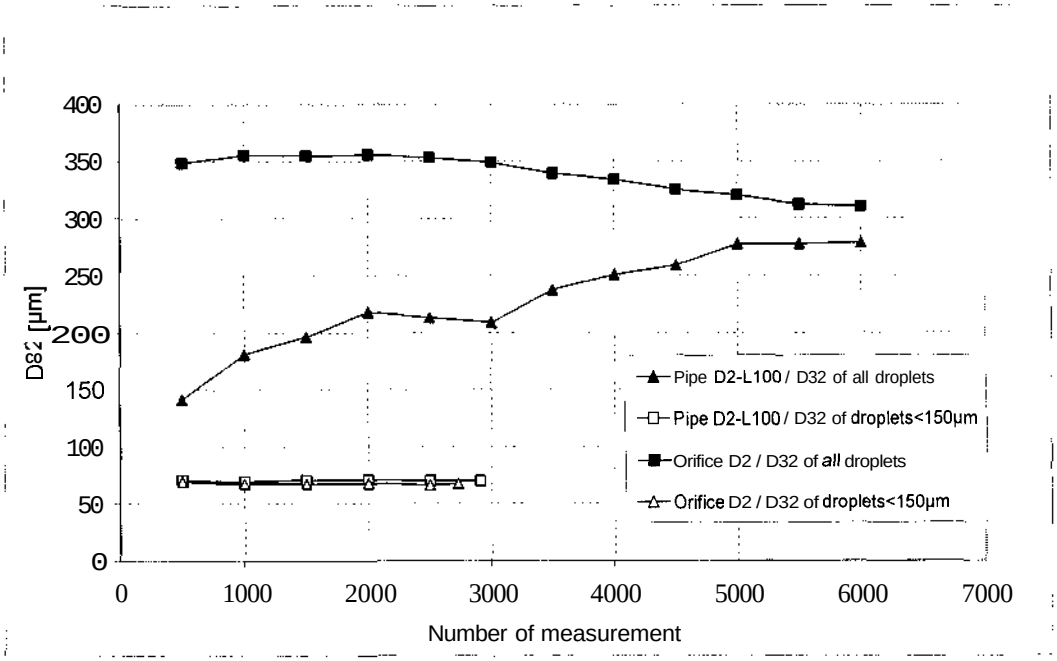

Fig 7.: d_{32} measurement accuracy versus droplet number (small droplets ; whole population).

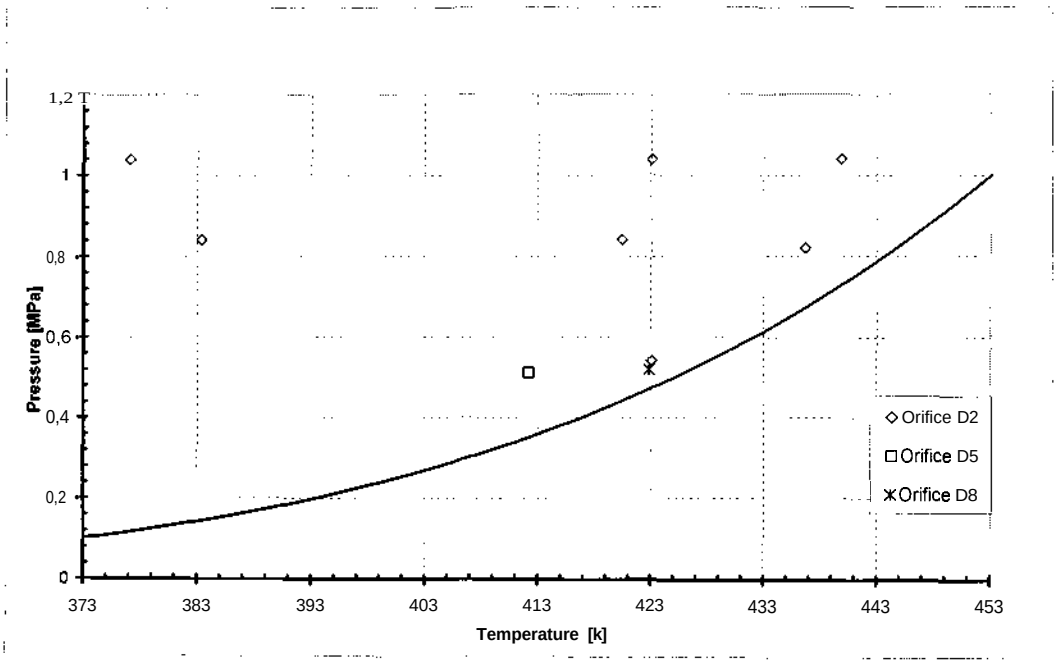

fig. 8.: Experimental reservoir conditions. Waterjets from orifices.

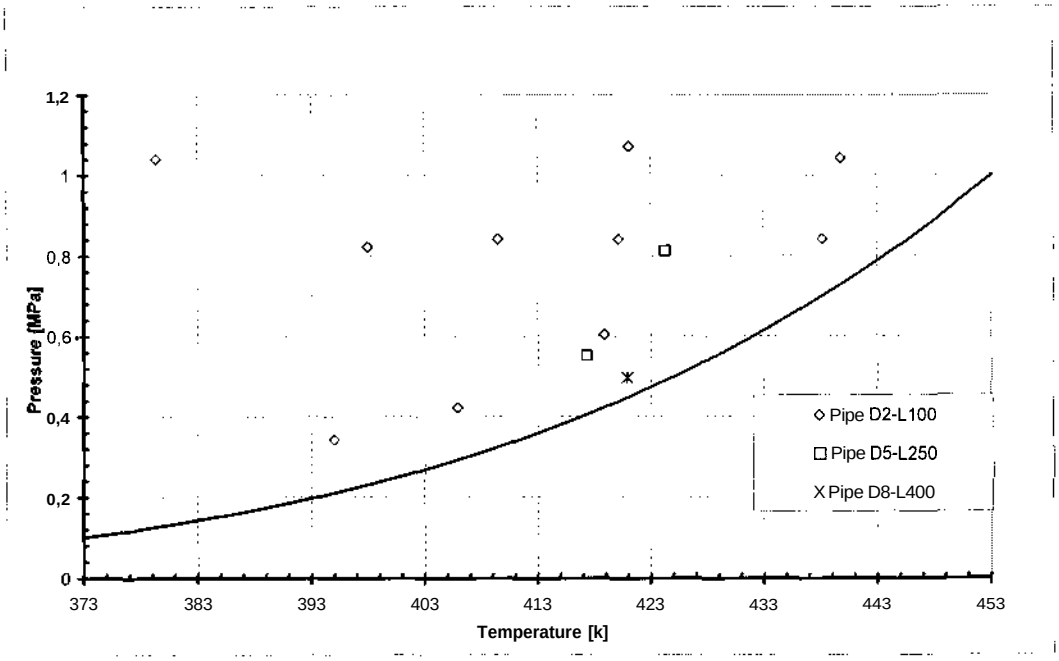

fig. 9.: Experimental reservoir conditions. Water jets from pipes.

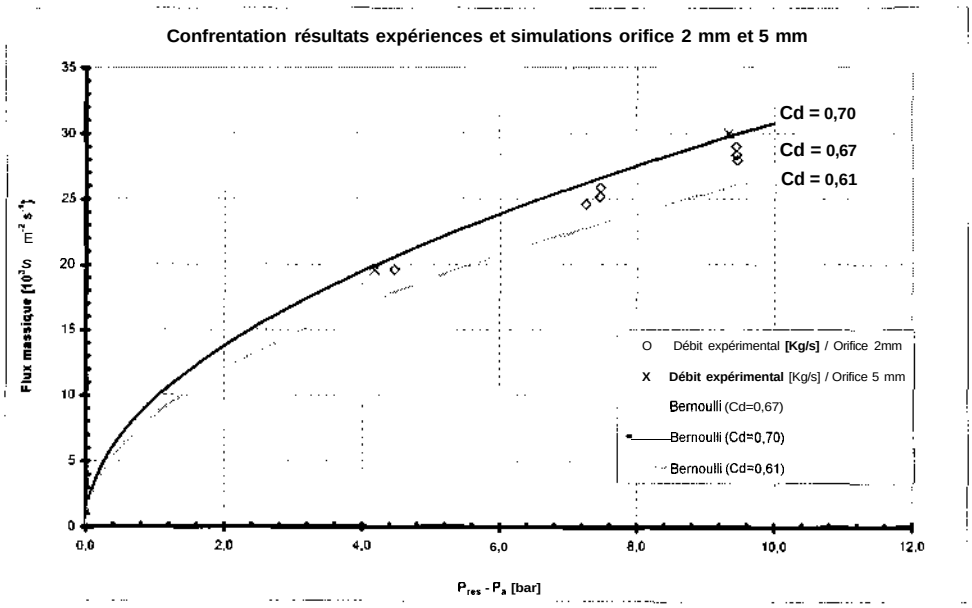

Figure 10. : Mass velocity versus relative réservoir pressure (orifices)

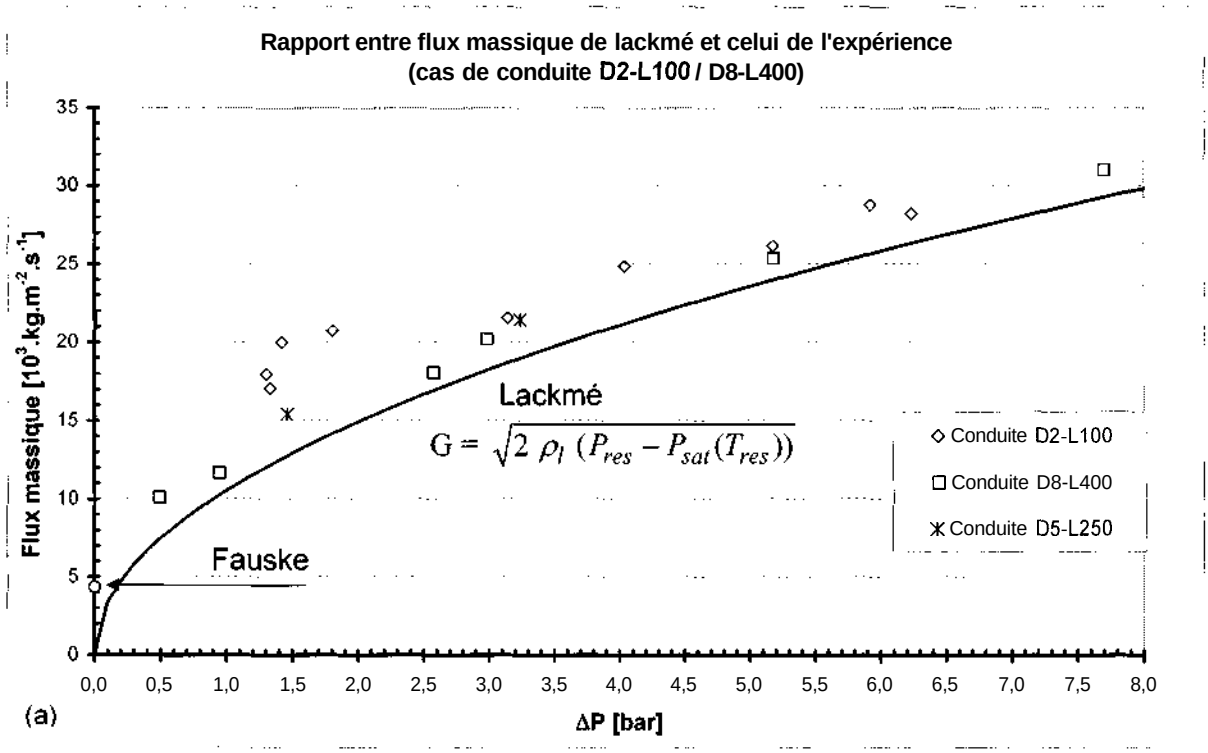

Fig 11. : mass velocity versus (P_{res} - P_{sat} (T_{res})) (pipes)

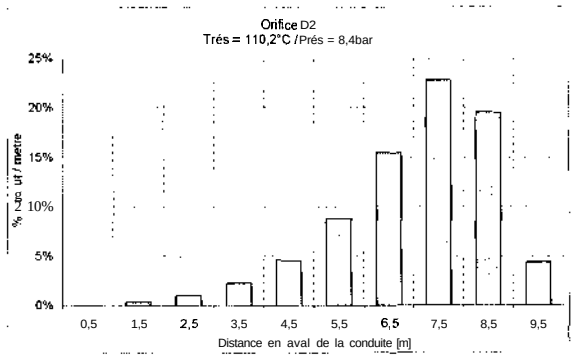

T_{res} = 110,2°C / $P_{rés}$ = 8,4bar

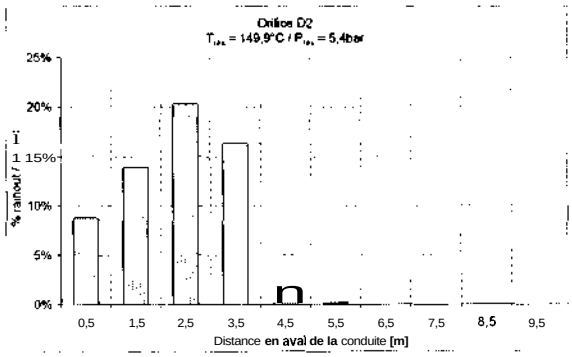

T_{res} = 149,9°C / $P_{rés}$ = 5,4bar

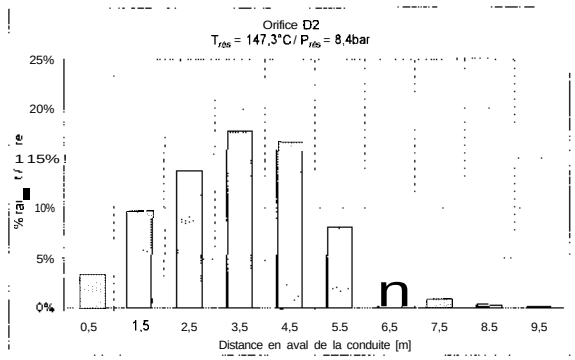

T_{res} = 147,3°C / $P_{rés}$ = 8,4bar

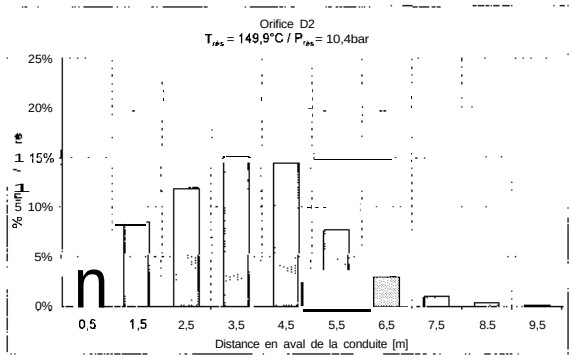

T_{res} = 149,9°C / $P_{rés}$ = 10,4bar

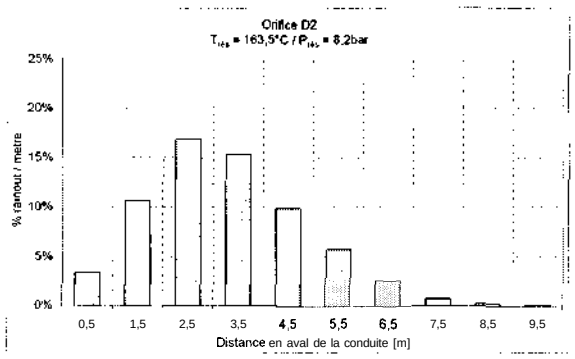

T_{res} = 163,5°C / $P_{rés}$ = 8,2bar

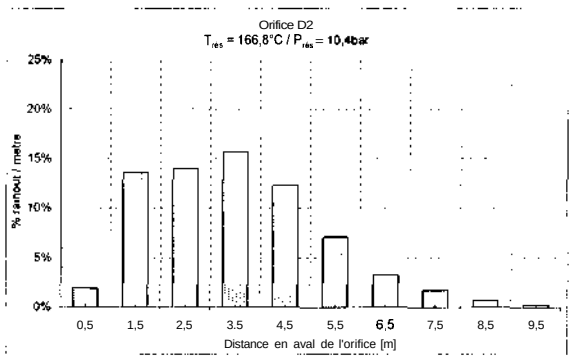

T_{res} = 166,7°C / $P_{rés}$ = 10,4bar

Fig 12. : Spatial distribution ofrain-out (D2 orifice).

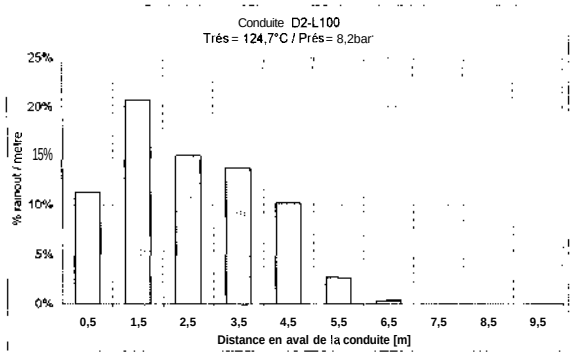

$T_{rés}$ = 124,7°C / $P_{rés}$ = 8,2bar

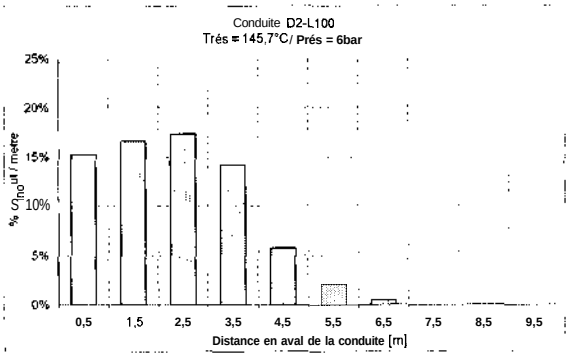

$T_{rés}$ = 145,7°C / $P_{rés}$ = 6bar

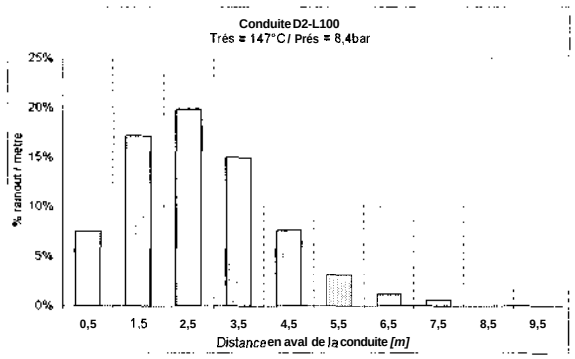

$T_{rés}$ = 147°C / $P_{rés}$ = 8,4bar

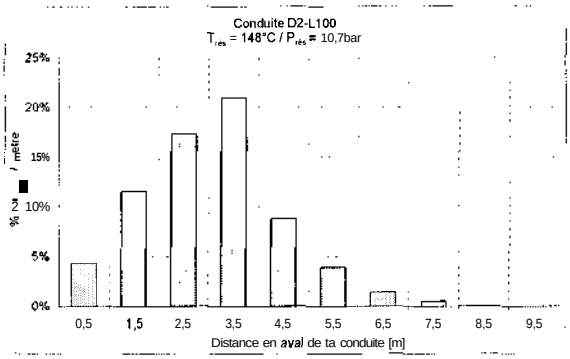

$T_{rés}$ = 148°C / $P_{rés}$ = 10,7bar

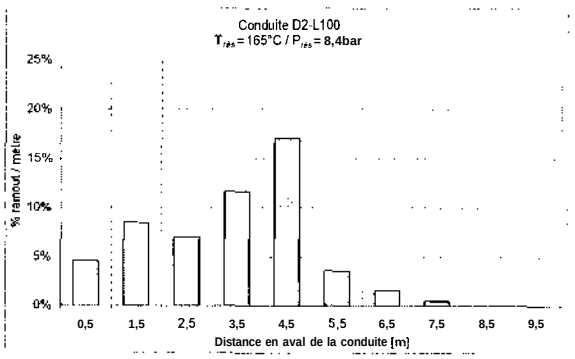

$T_{rés}$ = 165°C / $P_{rés}$ = 8,4bar

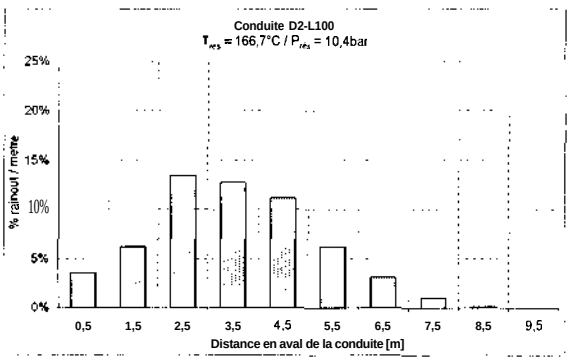

$T_{rés}$ = 166,7°C / $P_{rés}$ = 10,4bar

Fig 13. : Spatial distribution of rain-out (D2L100 pipe).

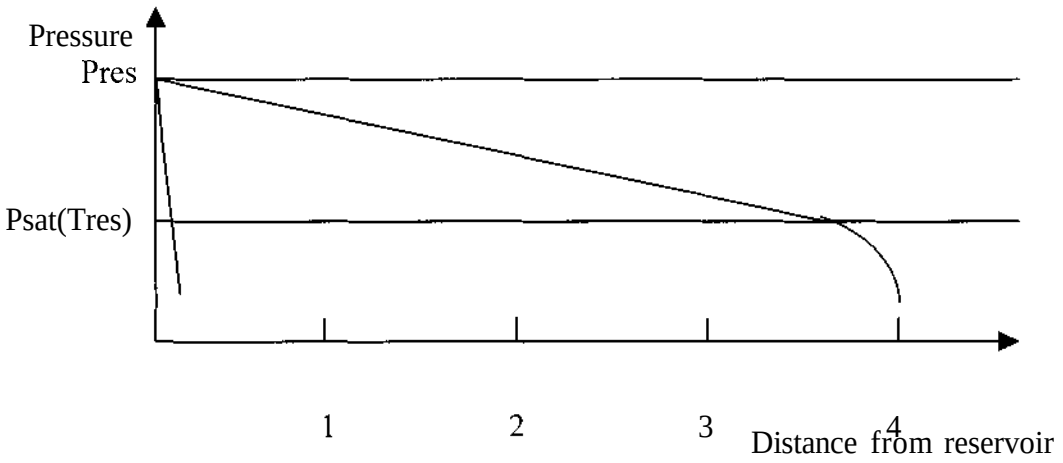

Fig. 14. : influence of pressure gradient on internal 2-phase flow structure

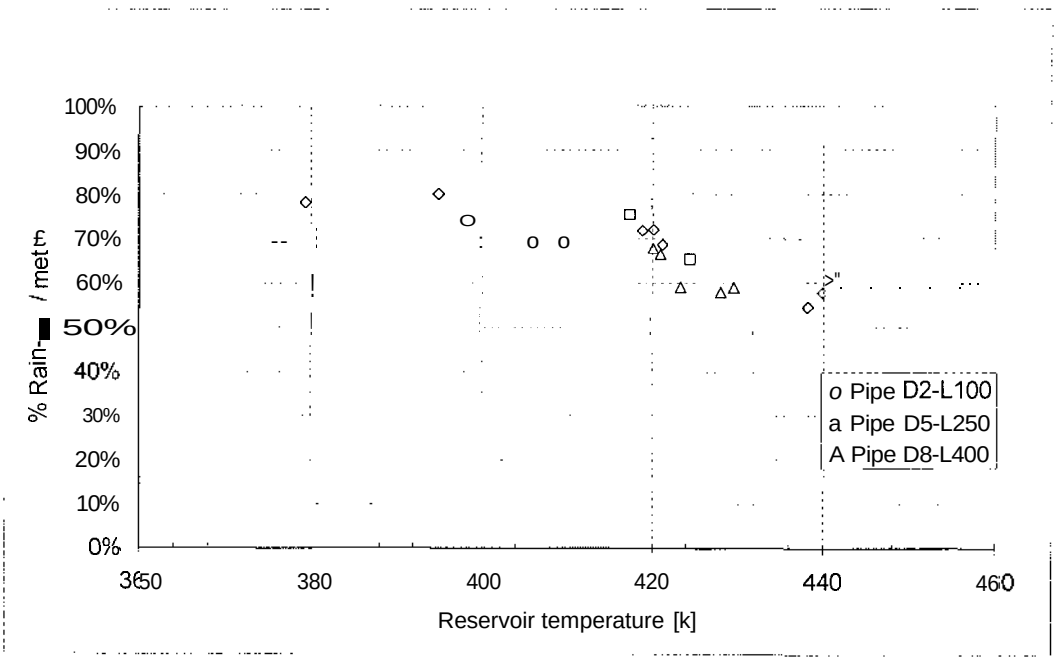

Fig. 15. : rain-out fraction versus réservoir température (pipes).

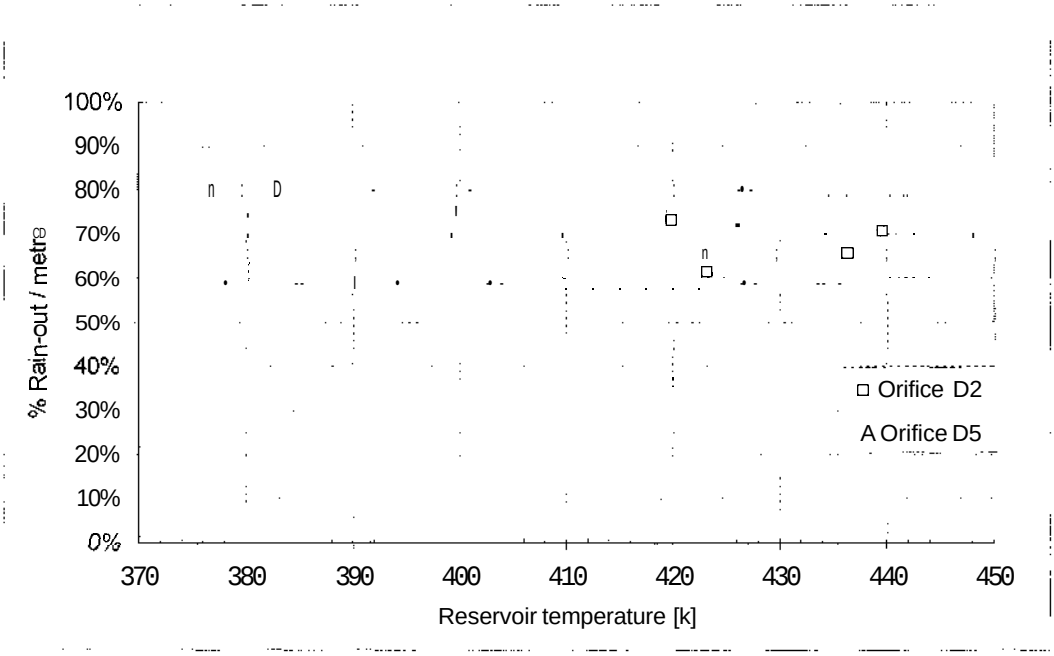

Fig. 16. : rain-out fraction versus reservoir temperature (orifices).

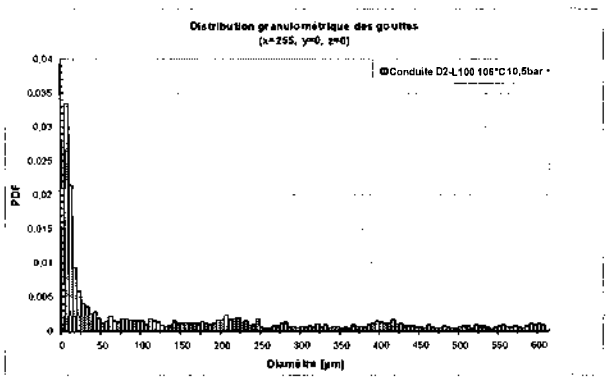

T_{res} = 106 °C / P_{res} = 10.5 bar

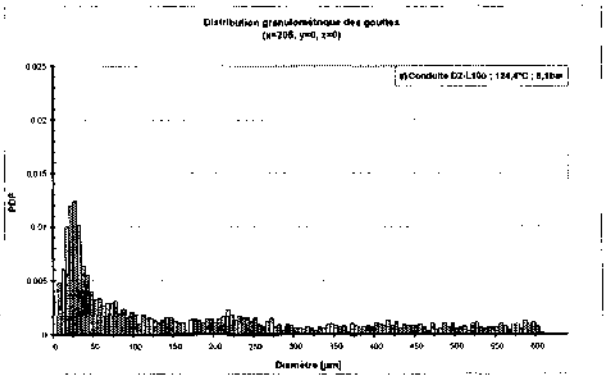

T_{res} = 124.4 °C / P_{res} = 8.1 bar

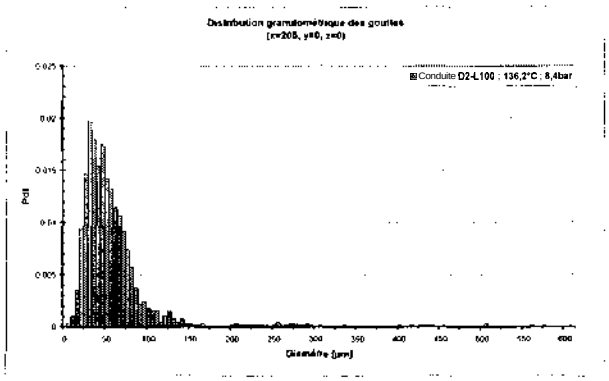

T_{res} = 136.2 °C / P_{res} = 8.4 bar

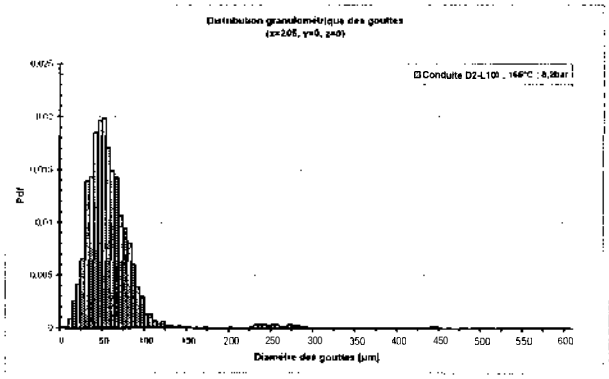

T_{res} = 165 °C / P_{res} = 8.2 bar

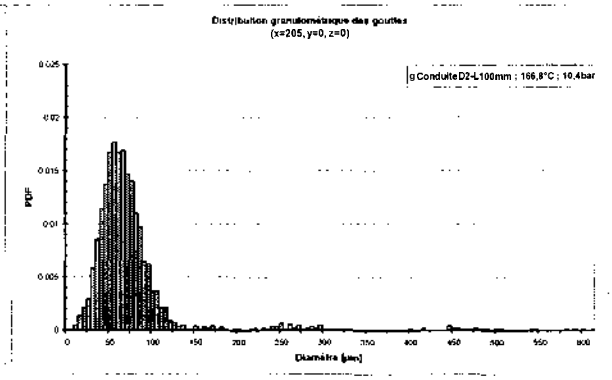

T_{res} = 166.8 °C / P_{res} = 10.4 bar

Fig. 17. : Number size distribution at différent reservoir conditions
(200 mm down-stream from D2L100 pipe)

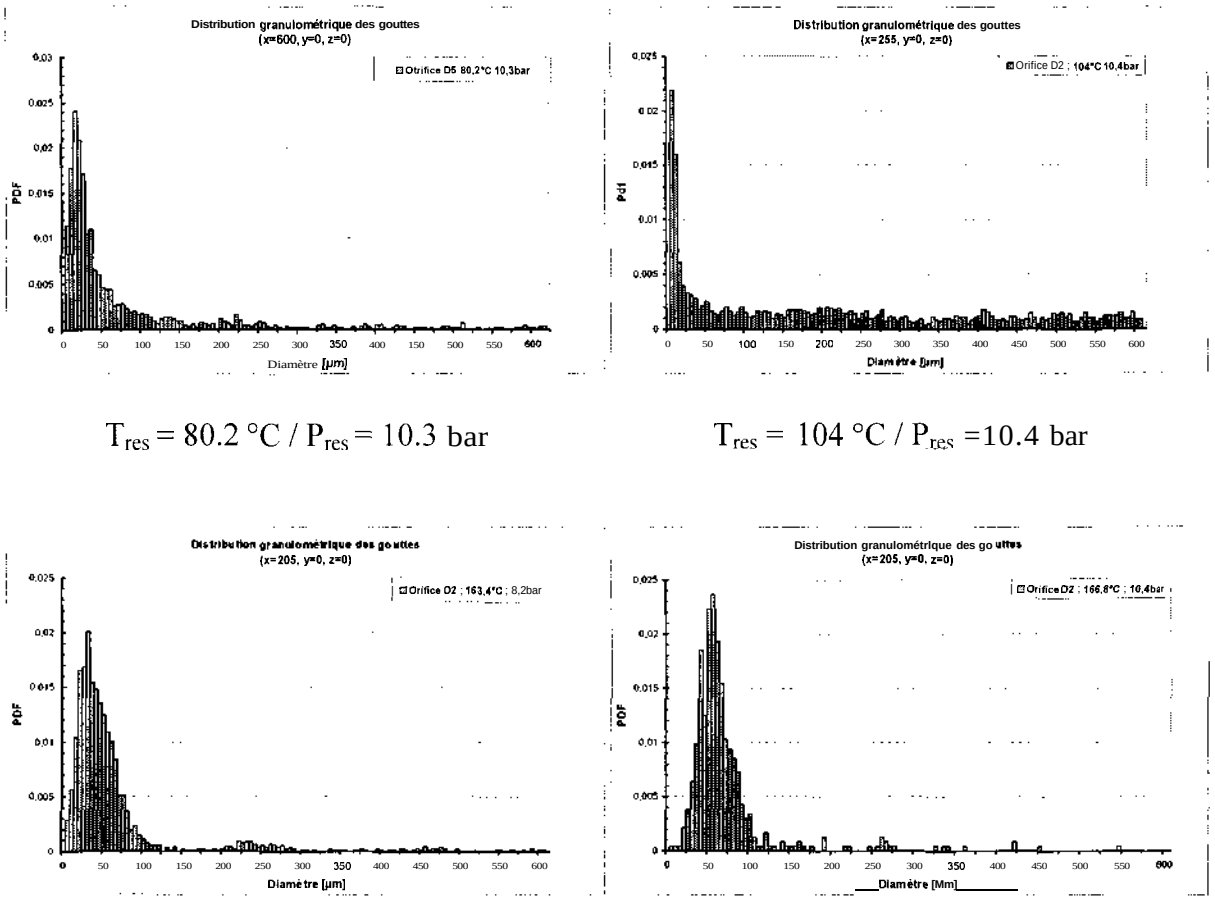

T_{res} = 80.2 °C / P_{res} = 10.3 bar

T_{res} = 104 °C / P_{res} =10.4 bar

T_{res} = 163.4 °C / P_{res} = 8.2 bar

T_{res} = 166.8 °C / P_{res} = 10.4 bar

Fig. 18.: Number size distribution at different reservoir conditions
(200 mm down-stream from D2 orifice)

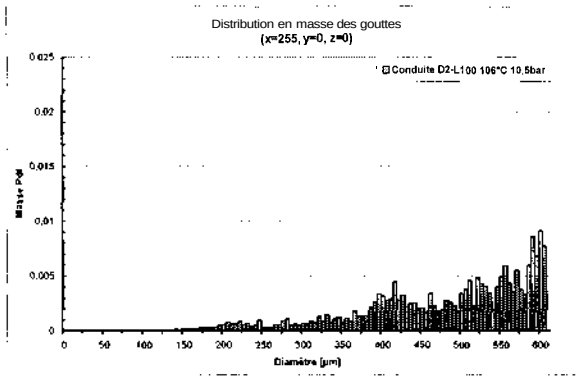

T_{res} = 106 °C / P_{res} =10.5 bar

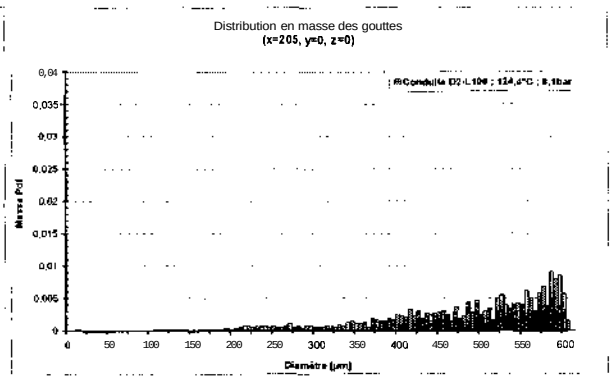

T_{res} = 124.4 °C / P_{res} = 8.1 bar

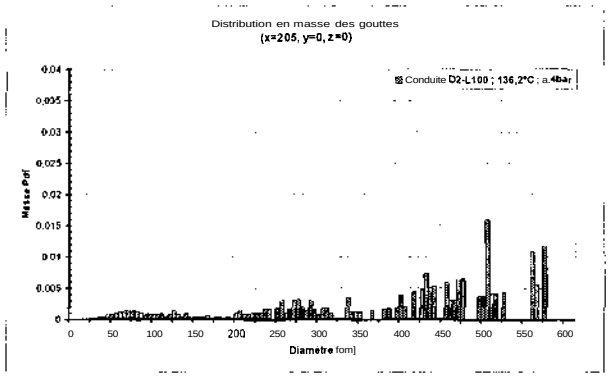

T_{res} = 136.2 °C / P_{res} = 8.4 bar

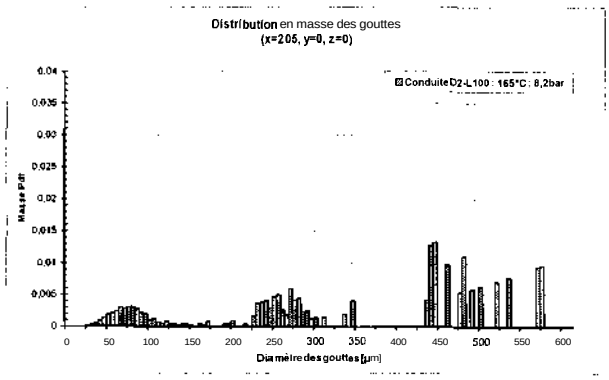

T_{res} = 165 °C / P_{res} = 8.2 bar

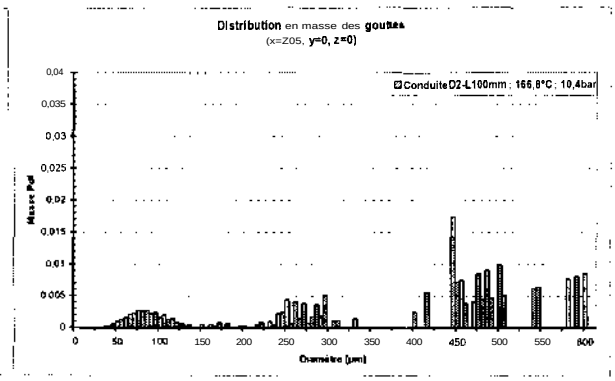

T_{res} = 166.8 °C / P_{res} = 10.4 bar

Fig. 19. : mass size distribution at different reservoir conditions
(200 mm down-stream from D2L100 pipe)

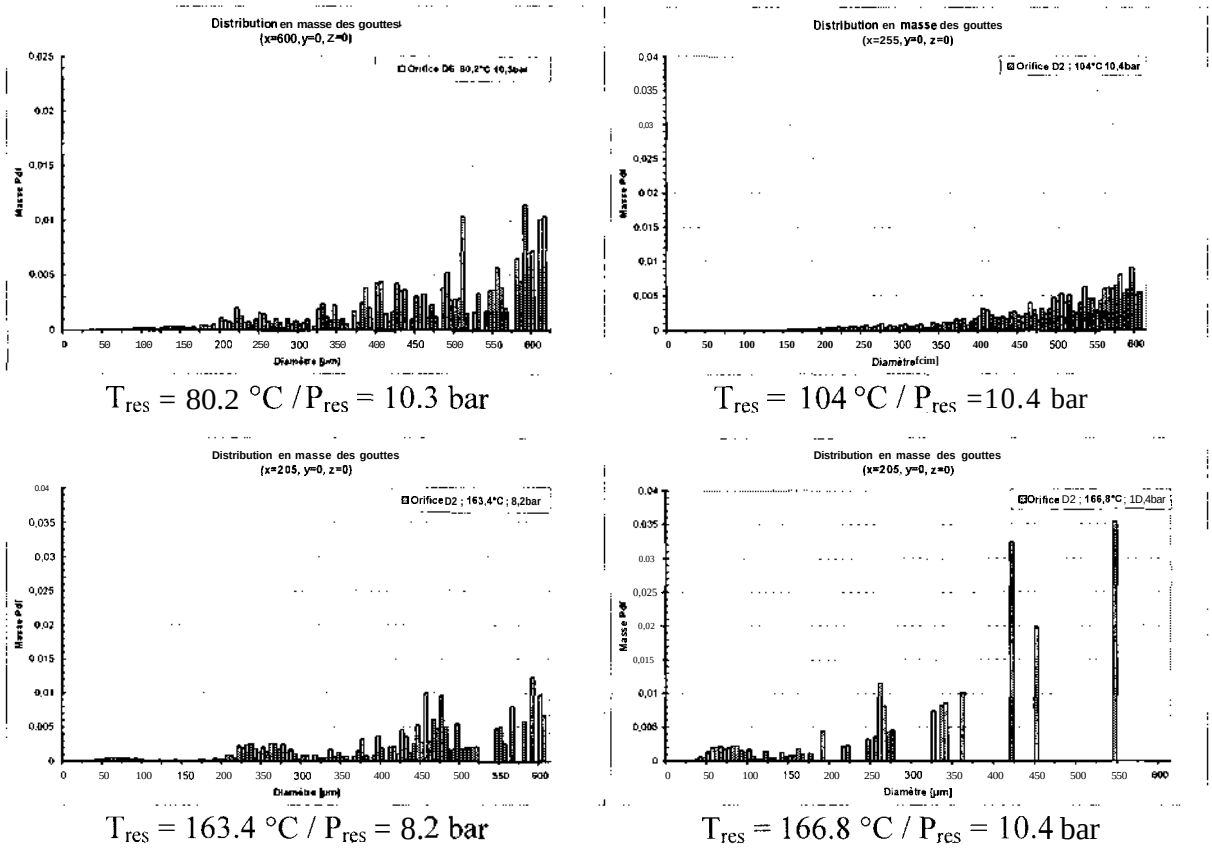

T_{res} = 80.2 °C / P_{res} = 10.3 bar

T_{res} = 104 °C / P_{res} =10.4 bar

T_{res} = 163.4 °C / P_{res} = 8.2 bar

T_{res} = 166.8 °C / P_{res} = 10.4 bar

Fig. 20. : mass size distribution at différent reservoir conditions
(200 mm down-stream from D2 orifice)

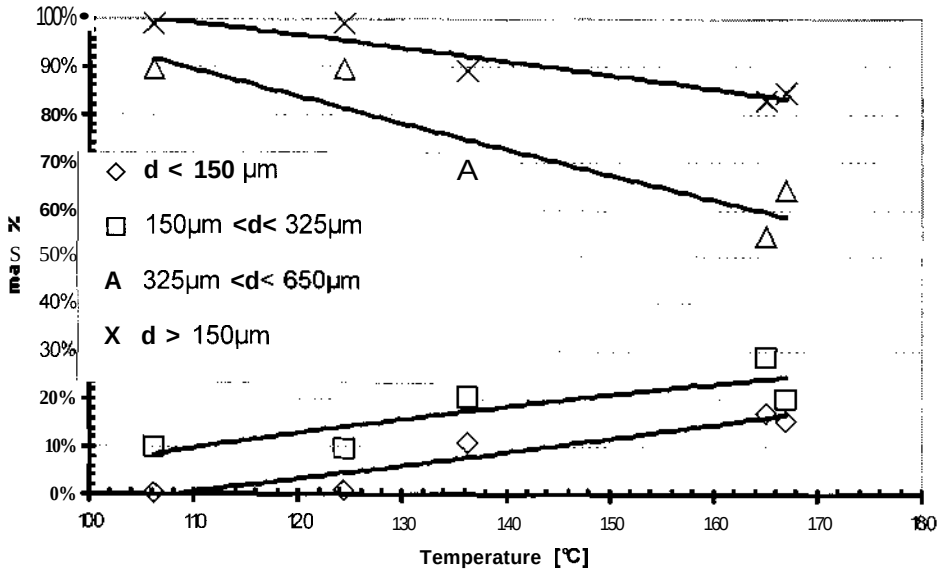

Fig. 21. : mass % of large droplets versus reservoir temperature

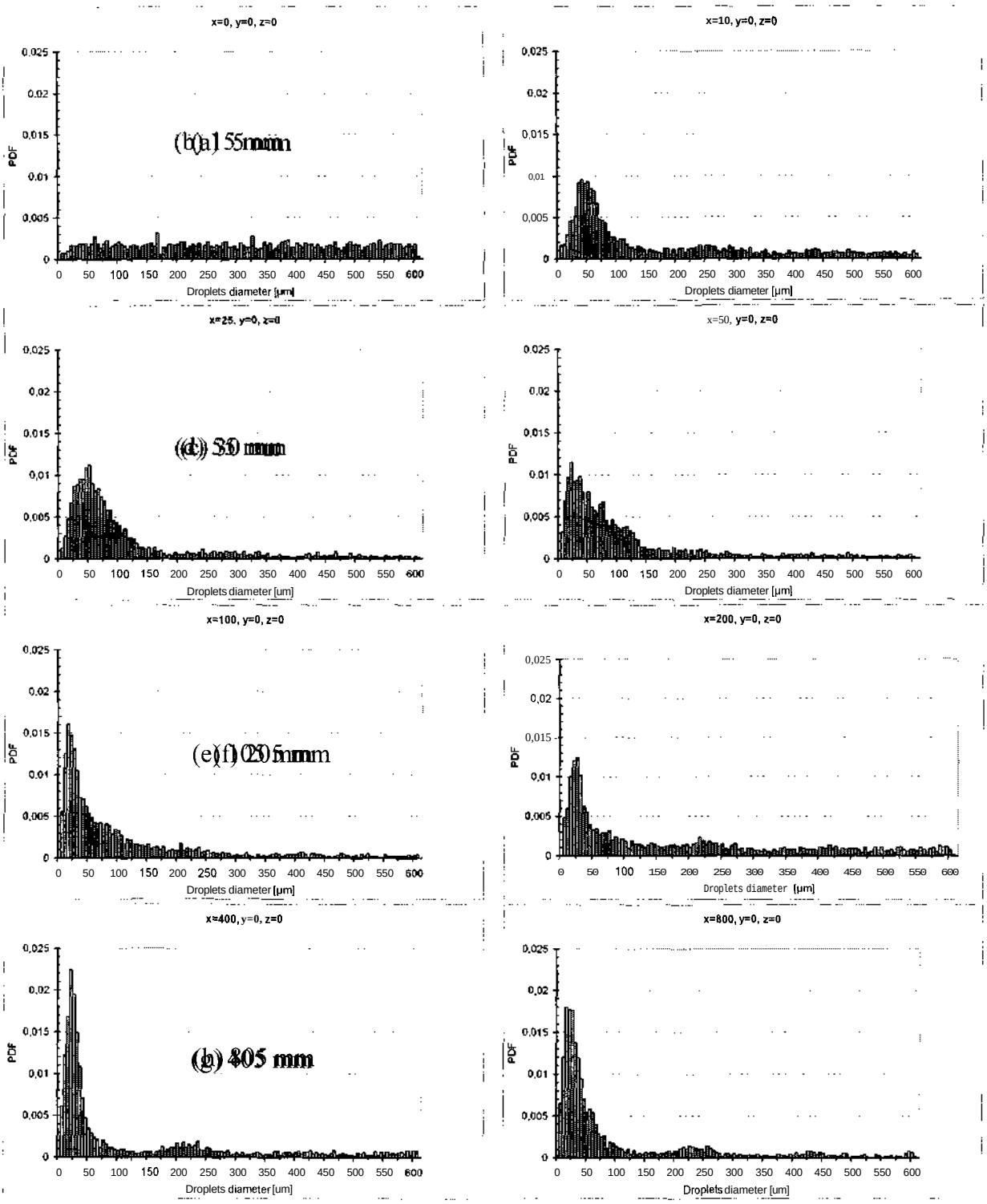

Fig. 22: number size distribution at different locations

(D2L100 pipe, T_{res} = 397K; P_{res} = .82 MPa)

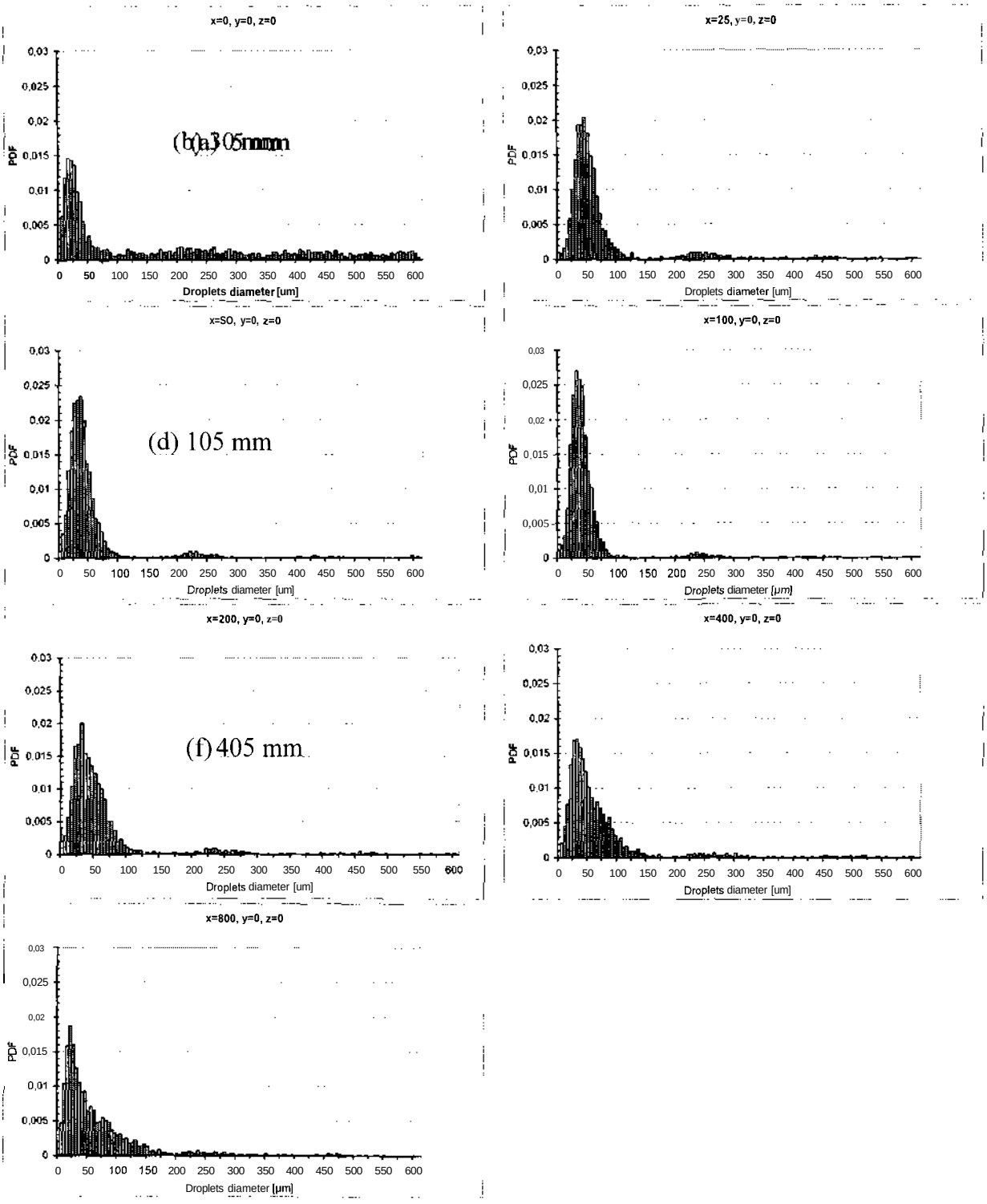

Fig. 23: number size distribution at different locations

(D2 orifice, T_{res} = 437K; P_{res} = .82 MPa)

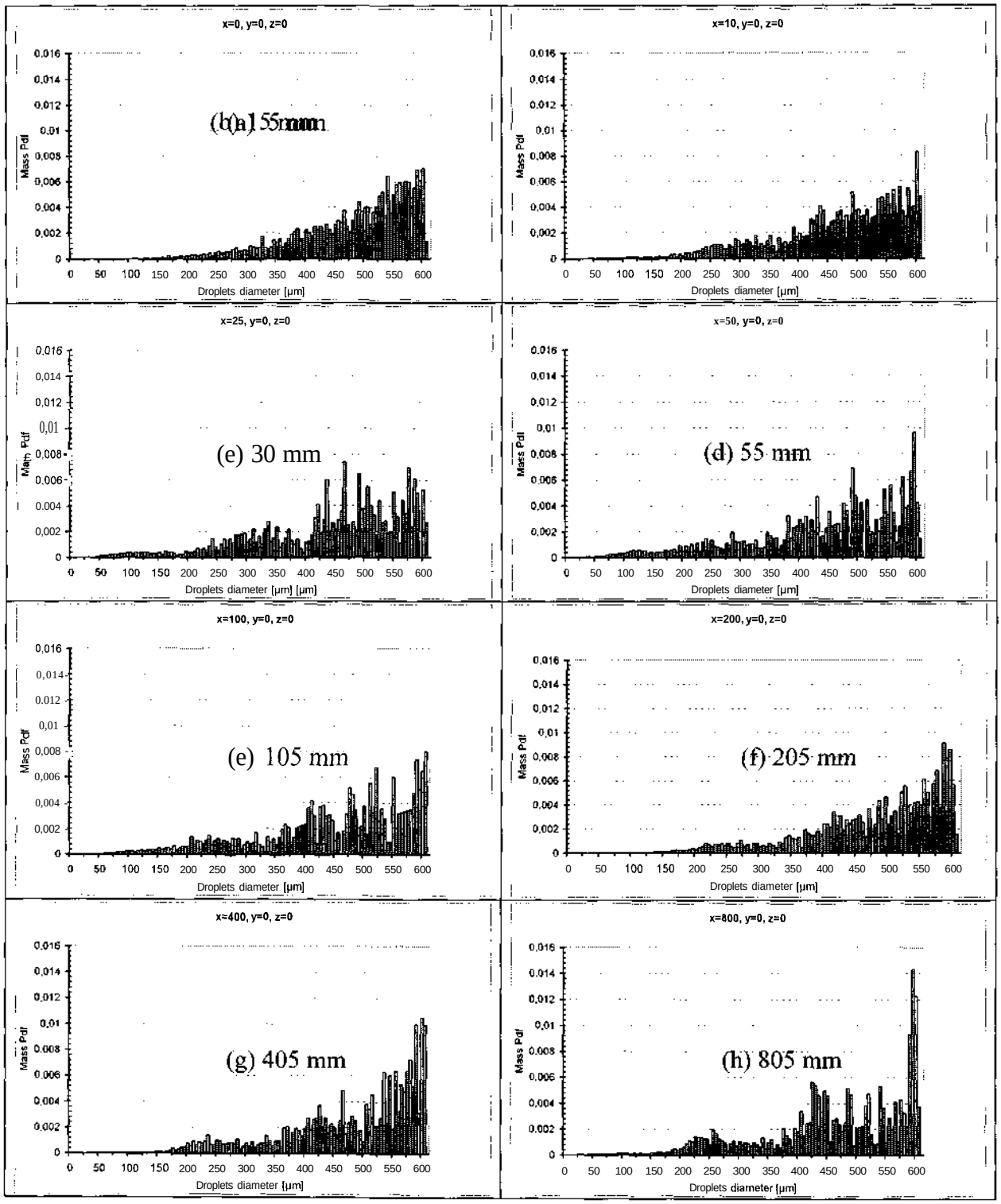

Fig. 24: mass size distribution at different locations

(D2L100 pipe, T_{res} = 397K; P_{res} = .82 MPa)

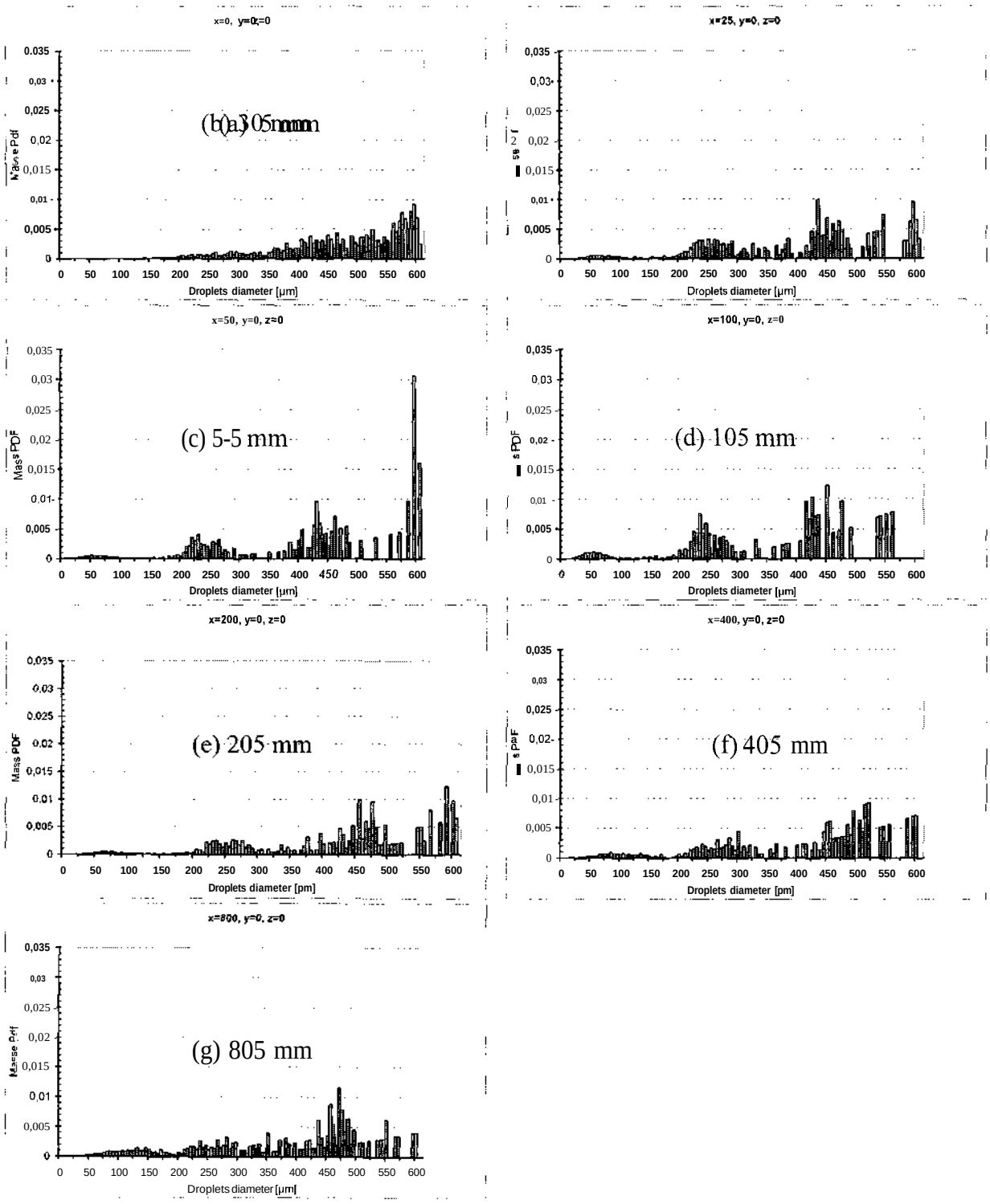

Fig. 25: mass size distribution at different locations

(D2 orifice, T_{res} = 437K; P_{res} = .82 MPa)

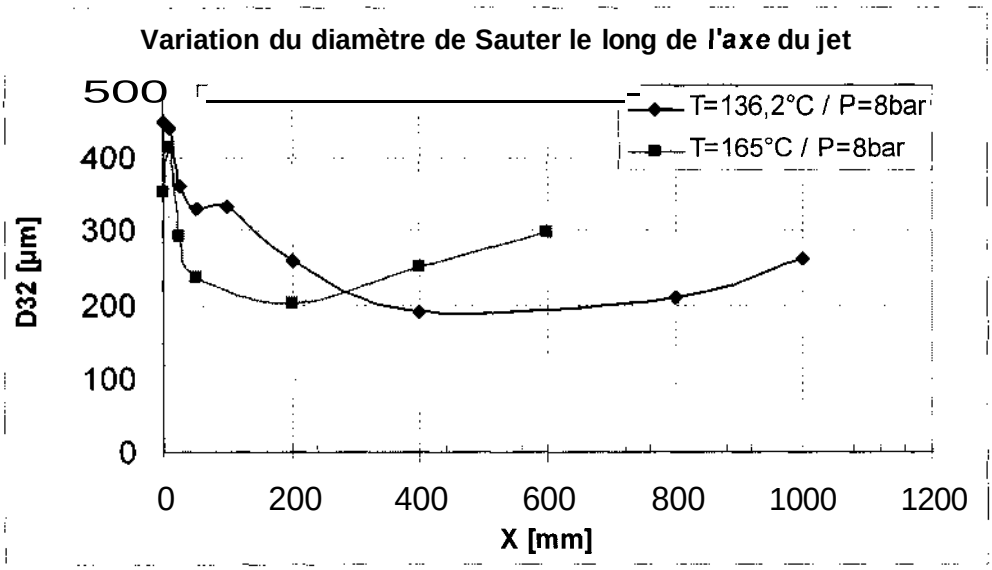

Fig. 26. : Change of mean SAUTER with distance from the pipe

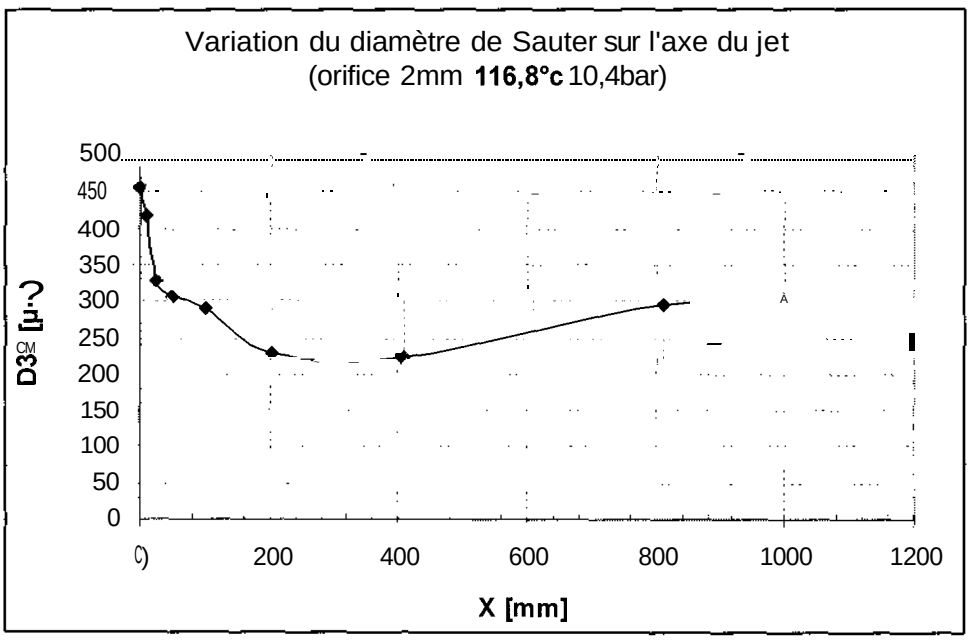

Fig. 27. : Change of mean SAUTER with distance from the orif